AIMS Mathematics, 10(6): 14996–15011.
DOI: 10.3934/math.2025672
Received: 19 April 2025
Revised: 14 June 2025
Accepted: 24 June 2025
Published: 30 June 2025

https://www.aimspress.com/journal/Math

Research article

Primary resonance analysis of a novel fractional-order coronary artery model

Guanghua Wei[1], **Xiaorong Zhang**[2] **and Zhoujin Cui**[3,*]

[1] School of Science, Jinling Institute of Technology, Nanjing, 211169, China
[2] School of Economics and Management, Jiangsu Maritime Institute, Nanjing, 211170, China
[3] School of Mathematical Sciences, Jiangsu Second Normal University, Nanjing, 210013, China

* **Correspondence:** Email: cuizhoujin@126.com.

Abstract: This paper analyzed the primary resonance of a novel fractional-order coronary artery model, exploring cardiovascular diseases related to vascular behavior from the nonlinear dynamics perspective. By applying the averaging method, approximate analytical solutions and the amplitude-frequency equation were derived, whereas Lyapunov stability theory was utilized to analyze the steady-state behavior. Numerical simulations validated the accuracy of the analytical approach, demonstrating close agreement between theoretical predictions and computational results. Key findings include the identification of parameter-driven bifurcations that modulate resonance amplitude and stability. Specifically, a lower fractional order q and reduced damping μ amplify resonant responses, while increased pulse pressure F correlates with elevated spasm risk. These results provide a theoretical framework for understanding how blood vessel viscoelasticity and external stimuli influence cardiovascular dynamics, offering insights for developing diagnostic tools and therapeutic strategies to mitigate coronary artery spasm and related cardiovascular diseases.

Keywords: fractional-order coronary artery model; primary resonance; averaging method; amplitude-frequency equation
Mathematics Subject Classification: 34A08, 34K37, 37N99

1. Introduction

Cardiovascular diseases (CVDs), including coronary artery spasm and myocardial infarction, are the leading global cause of death. Alarmingly, over 75% of related fatalities occur in low- and middle-income countries [1]. At the root of CVDs lies the impaired function of the heart or blood vessels, which disrupts the body's efficient physiological processes. The coronary arteries, specific branches of muscular blood vessels in the heart, share close associations with general muscular blood vessels

in structure, function, and pathological mechanisms. These arteries play a crucial role in delivering oxygen and nutrients to the heart muscle. However, they are highly susceptible to pathological changes, such as spasms. Coronary artery spasms, characterized by chaotic contractions, can severely disrupt blood flow, leading to life-threatening conditions like variant angina [2–4].

Given its critical significance, coronary artery research has captured the extensive attention in recent years. For example, Meng et al. found that there is at least one periodic solution in the biological mathematical model of muscular vessels, indicating that when such vessels are subjected to certain periodic stimuli, the biomathematical model can reveal their corresponding periodic variations [5]. Lin et al. [6] explored the nonlinear behavior and chaos suppression in a coronary artery chaotic system. Karimi et al. [7] numerically investigated the initiation and propagation of a crack in the intraluminal and radial locations of the healthy and atherosclerotic human coronary arterial walls. Carvalho et al. [8] reviewed recent numerical studies on coronary arteries, addressing blood viscosity models and physiological flow conditions. Ding et al. [9] investigated the chaos suppression of coronary artery systems and designed the smooth second-order sliding mode controller to suppress the chaos phenomenon. El Khaloufi et al. [10] addressed synchronization of pathological changes in coronary artery obstruction patients with nominal system models.

To date, most cardiovascular research models rely on integer-order calculus to describe vascular dynamics, providing a basic framework for arterial wall mechanics but failing to capture the complex viscoelastic properties of biological tissues—articularly the "memory" effects inherent to arterial walls. Fractional-order calculus addresses this gap by incorporating derivatives that mathematically model historical stress-strain dependencies and long-range memory in biological materials. This allows for more accurate representation of vascular tissues' layered structure and continuous relaxation behavior, which are unaccounted for in integer-order models. For instance, the investigations in [11–13] employed fractional calculus and fractional-order viscoelasticity to model the viscoelastic behavior of arteries. Researchers in [14–16] explored the application of fractional calculus in modeling diverse biological systems, highlighting its ability to capture complex dynamical behaviors in biological phenomena. The scholars in [17] replaced integer-order derivatives with fractional derivatives in a muscular blood vessel model to characterize its chaotic dynamics.

While coronary artery models have been widely studied, their resonant behaviors remain underexplored. As a key phenomenon where the system exhibits large-amplitude responses at specific excitation frequencies, in-depth analysis of primary resonance characteristics in the fractional-order coronary artery model helps reveal the potential pathogenesis of coronary artery diseases. The influence of fractional derivatives on nonlinear system dynamics, a burgeoning research area, has unveiled novel dynamic behaviors in fractional-order damped systems (see [18–22]). Motivated by these findings, this paper investigates the primary resonance of a novel fractional-order coronary artery model. Through meticulous analysis of the model's frequency response curves and the interplay between external excitation frequency and amplitude, we aim to clarify how the fractional-order parameter modulates the system's amplitude-frequency characteristics. These insights are expected to advance our understanding of coronary artery biomechanics.

The paper is organized as follows: In Section 2, the amplitude-frequency equation for primary resonance is derived, along with conditions that determine the stability of the steady-state solution. Section 3 presents different types of amplitude-frequency curves. The utility of the amplitude-frequency equation for estimating primary resonant solutions is numerically validated in Section 4.

Finally, concluding remarks are provided in Section 5.

2. Primary resonance

2.1. Fractional-order coronary artery model

The work in [5, 6] showed that the coronary artery system can be mathematically modeled as

$$\begin{cases} \dfrac{\mathrm{d}x}{\mathrm{d}t} = -by - cx, \\ \dfrac{\mathrm{d}y}{\mathrm{d}t} = \lambda(-x + x^3 - y) + \lambda\dfrac{\mathrm{d}x}{\mathrm{d}t}, \end{cases} \tag{2.1}$$

where x denotes the change in the inner radius of the vessel, y is the pressure change in the vessel, t is the non-dimensional time variable, and λ, b, c are the coronary artery system parameters. Equation (2.1) can be written as

$$\frac{\mathrm{d}^2x}{\mathrm{d}t^2} = (b\lambda - c\lambda)x - b\lambda x^3 - (\lambda + b\lambda + c)\frac{\mathrm{d}x}{\mathrm{d}t}.$$

Let $\mu = \lambda + b\lambda + c$, $\alpha = c\lambda - b\lambda$, $\gamma = b\lambda$. The disturbance term $F\cos\omega t$ is then introduced. In a biological context, this term can be interpreted as the periodic stimulation of blood vessels. Thus, the integer-order coronary artery model as reported in [5] is described through the following Duffing equation,

$$\ddot{x} + \mu\dot{x} + \alpha x + \gamma x^3 = F\cos\omega t, \tag{2.2}$$

where x denotes the change difference of vessel diameter, $F\cos\omega t$ can be explained as a periodic stimulation of blood vessels, and α, μ, γ are positive constants related to the blood flow resistance and the elasticity of the vessel wall.

The integer-order coronary artery model (2.2) effectively describes basic blood flow dynamics but overlooks the history-dependent viscoelasticity of arterial walls. Soft biological tissues, such as arterial walls, exhibit non-local behavior, which is incompatible with integer-order calculus. Fractional-order derivatives, defined via the Caputo operator $D_t^q x(t)$, address this limitation by incorporating a history-dependent integral term:

$$D_t^q x(t) = \frac{1}{\Gamma(1-q)}\int_0^t \dot{x}(\tau)(t-\tau)^{-q}\mathrm{d}\tau,$$

in which $\Gamma(z)$ is the Gamma function satisfying $\Gamma(z+1) = z\Gamma(z)$.

The fractional derivative is introduced to describe the structure of the arterial wall, and the constitutive equation describing the stress-strain relationship can be expressed as [23, 24]

$$\sigma(t) = \eta D_t^q \varepsilon(t),$$

where $\sigma(t)$ and $\varepsilon(t)$ represent stress and strain, respectively, and $0 < q < 1$. This formulation mimics the arterial wall's ability to "remember" past stresses, making it suitable for modeling viscoelastic phenomena like stress relaxation and creep.

By replacing the integer-order damping term $\mu\dot{x}$ with $\mu D_t^q x$, the proposed fractional-order model (2.3) captures the memory-dependent nature of arterial mechanics, providing a more realistic

representation of blood vessel behavior under pulsatile flow. The new model to describe the coronary artery is proposed as follows:

$$\ddot{x} + \mu D_t^q x + \alpha x + \gamma x^3 = F \cos \omega t. \tag{2.3}$$

This modification is crucial because clinical observations show that arterial wall dysfunction, such as reduced elasticity in atherosclerosis, strongly correlates with abnormal viscoelastic properties. Fractional-order calculus bridges the gap between mathematical modeling and biological reality, offering a robust framework to study how historical mechanical loads influence current cardiovascular health.

2.2. Amplitude-frequency equation

The averaging method, a useful tool for finding approximate solutions to nonlinear differential equations, simplifies these complex equations by replacing them with a more manageable averaged system: It integrates the right-hand side over a period or cycle and uses this average to form new equations that capture the original system's long-term, slow-varying behavior, making it easier to analyze aspects like stability, periodic solutions, and overall dynamics [25–27]. As a simple yet accurate model derived this way offers reference value for general system stability decisions, we will use it in this section to study related problems.

Using the coordinates transformation (this transformation satisfies, formally, the averaging method requirement) as follows:

$$\varepsilon\mu_1 = \mu, \omega_0 = \sqrt{\alpha}, \varepsilon\gamma_1 = \gamma, \varepsilon f = F,$$

Equation (2.3) becomes

$$\ddot{x} + \varepsilon\mu_1 D_t^q x + \omega_0^2 x + \varepsilon\gamma_1 x^3 = \varepsilon f \cos \omega t, \tag{2.4}$$

where ω_0 is the natural frequency. In this transformation, μ_1, γ_1, f are dimensionless quantities, and the transformation is only to satisfy the requirement of the averaging method formally. The primary resonance means the excitation frequency is close to the natural one, i.e., $\omega \approx \omega_0$, and we have:

$$\omega^2 = \omega_0^2 + \varepsilon\sigma,$$

where σ is the detuning factor. Equation (2.4) can be rewritten in the following form:

$$\ddot{x} + \omega^2 x = \varepsilon[f \cos \omega t - \mu_1 D_t^q x + \sigma x - \gamma_1 x^3]. \tag{2.5}$$

Suppose Eq (2.5) has the solution as

$$x(t) = a \cos \varphi, \quad \dot{x}(t) = -\omega a \sin \varphi,$$

where the amplitude a and the generalized phase $\varphi(\varphi = \omega t + \theta)$ are slow varying functions of t. In accordance with the averaging method, one could obtain:

$$\dot{a} = \frac{-1}{\omega}[P_1(a, \theta) + P_2(a, \theta)] \sin \varphi, \tag{2.6a}$$

$$a\dot{\theta} = \frac{-1}{\omega}[P_1(a, \theta) + P_2(a, \theta)] \cos \varphi, \tag{2.6b}$$

where

$$P_1(a,\theta) = \varepsilon[f\cos(\varphi-\theta) + \sigma a\cos\varphi - \gamma_1 a^3\cos^3\varphi], \tag{2.7a}$$

$$P_2(a,\theta) = -\varepsilon\mu_1 D_t^q(a\cos\varphi). \tag{2.7b}$$

Moreover, one could apply the standard averaging method [25–27] to Eqs (2.7a) and (2.7b) in time interval $[0,T]$, which means

$$\dot{a} = \frac{-1}{T\omega}\int_0^T [P_1(a,\theta) + P_2(a,\theta)]\sin\varphi \mathrm{d}\varphi, \tag{2.8a}$$

$$a\dot{\theta} = \frac{-1}{T\omega}\int_0^T [P_1(a,\theta) + P_2(a,\theta)]\cos\varphi \mathrm{d}\varphi. \tag{2.8b}$$

Based on the averaging method, one could select the time terminal T as $T = 2\pi$ if $P_i(a,\theta)(i = 1,2)$ is a periodic function, or $T = \infty$ if $P_i(a,\theta)(i = 1,2)$ is an aperiodic one. Thus, the simplified forms of the first term of Eqs (2.8a) and (2.8b) would be:

$$\dot{a}_1 = \frac{-1}{2\pi\omega}\int_0^{2\pi} P_1(a,\theta)\sin\varphi \mathrm{d}\varphi = -\frac{\varepsilon f}{2\omega}\sin\theta, \tag{2.9a}$$

$$a\dot{\theta}_1 = \frac{-1}{2\pi\omega}\int_0^{2\pi} P_1(a,\theta)\cos\varphi \mathrm{d}\varphi = -\frac{\varepsilon f}{2\omega}\cos\theta - \frac{\varepsilon\sigma a}{2\omega} + \frac{3\varepsilon\gamma_1 a^3}{8\omega}. \tag{2.9b}$$

Substitute Eq (2.7b) into Eqs (2.8a) and (2.8b). When $0 < q < 1$, the second part of these equations can be calculated as:

$$\dot{a}_2 = -\lim_{T\to\infty}\frac{1}{T\omega}\int_0^T P_2(a,\theta)\sin\varphi \mathrm{d}\varphi = \lim_{T\to\infty}\frac{-\varepsilon\mu_1 a}{T\Gamma(1-q)}\int_0^T\{\int_0^t \frac{\sin(\omega\tau+\theta)}{(t-\tau)^q}d\tau\}\sin\varphi \mathrm{d}\varphi, \tag{2.10a}$$

$$a\dot{\theta}_2 = -\lim_{T\to\infty}\frac{1}{T\omega}\int_0^T P_2(a,\theta)\cos\varphi \mathrm{d}\varphi = \lim_{T\to\infty}\frac{-\varepsilon\mu_1 a}{T\Gamma(1-q)}\int_0^T\{\int_0^t \frac{\sin(\omega\tau+\theta)}{(t-\tau)^q}d\tau\}\cos\varphi \mathrm{d}\varphi. \tag{2.10b}$$

Two important integral formulas from [19] are used in Eqs (2.10a) and (2.10b),

$$\lim_{T\to\infty}\int_0^T \frac{\sin(\omega t)}{t^q}\mathrm{d}t = \omega^{q-1}\Gamma(1-q)\cos(\frac{q\pi}{2}), \tag{2.11a}$$

$$\lim_{T\to\infty}\int_0^T \frac{\cos(\omega t)}{t^q}\mathrm{d}t = \omega^{q-1}\Gamma(1-q)\sin(\frac{q\pi}{2}), \tag{2.11b}$$

and we can get

$$\dot{a}_2 = -\frac{\varepsilon\mu_1 a\omega^{q-1}}{2}\sin(\frac{q\pi}{2}), \tag{2.12a}$$

$$a\dot{\theta}_2 = \frac{\varepsilon\mu_1 a\omega^{q-1}}{2}\cos(\frac{q\pi}{2}). \tag{2.12b}$$

From Eqs (2.9a), (2.9b), (2.12a), and (2.12b), Eqs (2.8a) and (2.8b) can be expressed as

$$\dot{a} = -\frac{\varepsilon f}{2\omega}\sin\theta - \frac{\varepsilon\mu_1 a\omega^{q-1}}{2}\sin(\frac{q\pi}{2}), \tag{2.13a}$$

$$a\dot{\theta} = -\frac{\varepsilon f}{2\omega}\cos\theta - \frac{\varepsilon\sigma a}{2\omega} + \frac{3\varepsilon\gamma_1 a^3}{8\omega} + \frac{\varepsilon\mu_1 a\omega^{q-1}}{2}\cos(\frac{q\pi}{2}). \tag{2.13b}$$

Substituting the parameters with the original ones, Eqs (2.13a) and (2.13b) become

$$\dot{a} = -\frac{F}{2\omega}\sin\theta - \frac{a}{2}C(q), \tag{2.14a}$$

$$a\dot{\theta} = -\frac{F}{2\omega}\cos\theta + \frac{a}{2\omega}[-\omega^2 + K], \tag{2.14b}$$

where

$$K = \alpha + \frac{3\gamma a^2}{4} + K(q),$$

$$K(q) = \mu\omega^q\cos(\frac{q\pi}{2}),$$

$$C(q) = \mu\omega^{q-1}\sin(\frac{q\pi}{2}).$$

We define these two combined parameters as the equivalent damping coefficient and equivalent stiffness coefficient of Eq (2.2). When $q = 1$, we can get $K(q) = 0$, $C(q) = \mu$. Notably, the fractional order q is a critical parameter governing the system's dynamics. The results indicate that q influences the system through power and trigonometric functions in the analytical solution, enabling the derivation of an approximate solution for the system.

The steady-state solution is studied which is an important achievement in vibration engineering. Let $\dot{a} = 0$ and $a\dot{\theta} = 0$.

When $0 < q < 1$, from Eqs (2.14a) and (2.14b), we have

$$F\sin\bar{\theta} = -\omega\bar{a}C(q), \tag{2.15a}$$

$$F\cos\bar{\theta} = -\omega^2\bar{a} + \bar{a}K, \tag{2.15b}$$

in which $\bar{a}$ and $\bar{\theta}$ are the steady-state amplitude and phase, respectively.

Eliminating $\bar{\theta}$ from Eqs (2.15a) and (2.15b), one could obtain the amplitude-frequency equation as

$$\bar{a}^2\{\omega^2[C(q)]^2 + [\omega^2 - K]^2\} = F^2, \tag{2.16}$$

and the phase-frequency equation as

$$\bar{\theta} = \arctan[\frac{\omega C(q)}{\omega^2 - K}]. \tag{2.17}$$

The maximum steady amplitude is

$$\bar{a}_{\max} = \frac{F}{\omega C(q)}, \tag{2.18}$$

which is related to the equivalent damping coefficient and exists at the excitation frequency

$$\omega = \sqrt{K}$$

that is related to the equivalent stiffness coefficient. The results obtained from Eqs (2.16)–(2.18) exhibit excellent consistency with the findings reported in [19]. Notably, when $q = 1$, the result derived from Eq (2.16) aligns exactly with the integer-order model presented in [32], illustrating the model's capability to degenerate into the classical integer-order case under specific conditions.

2.3. Stability of the steady resonant solutions

In the final part of this section, we analyze the stability of the steady-state solutions using Lyapunov stability theory. Lyapunov stability theory is a mathematical framework used to analyze the stability of dynamical systems, particularly for determining whether solutions to differential equations converge to an equilibrium point over time. Developed by Aleksandr Lyapunov in the late 19th century, the theory offers two primary approaches: Lyapunov's first method (indirect method) and Lyapunov's second method (direct method) [31]. Below, we employ Lyapunov's first method, which involves linearizing the system around an equilibrium point and analyzing the eigenvalues of the resulting Jacobian matrix. If all eigenvalues have negative real parts, the equilibrium is asymptotically stable. If any eigenvalue has a positive real part, the equilibrium is unstable. If eigenvalues have zero real parts, additional analysis (such as center manifold theory) is needed to determine stability.

The steady-state solution can be expressed as

$$x_s = \bar{a}\sin(\omega t + \bar{\theta}),$$

in which $\bar{a}$ and $\bar{\theta}$ satisfy Eqs (2.15a) and (2.15b). The small perturbations near the periodic motion x_s can be assumed as Δa and $\Delta\theta$. Let $a = \bar{a} + \Delta a$, $\theta = \bar{\theta} + \Delta\theta$. Substituting them into Eqs (2.14a) and (2.14b), ignoring higher-order terms, yields

$$\frac{d\Delta a}{dt} = -\frac{F}{2\omega}\cos\bar{\theta}\Delta\theta - \frac{C(q)}{2}\Delta a, \tag{2.19a}$$

$$\frac{d\Delta\theta}{dt} = (\frac{3\gamma\bar{a}}{4\omega} + \frac{F\cos\bar{\theta}}{2\omega\bar{a}^2})\Delta a + \frac{F}{2\omega\bar{a}}\sin\bar{\theta}\Delta\theta. \tag{2.19b}$$

Eliminating $\bar{\theta}$ from Eqs (2.19a) and (2.19b) based on Eqs (2.15a) and (2.15b), the characteristic determinant can be obtained as

$$\det\begin{vmatrix} -A_1 - \lambda & -\frac{\bar{a}}{2}A_2 \\ \frac{1}{2\bar{a}}A_3 & -A_1 - \lambda \end{vmatrix} = 0, \tag{2.20}$$

in which $A_1 = \frac{C(q)}{2}$, $A_2 = \frac{3\gamma\bar{a}^2}{4\omega} - \omega + \frac{K(q)}{\omega}$, $A_3 = \frac{9\gamma\bar{a}^2}{4\omega} - \omega + \frac{K(q)}{\omega}$.

Expanding the determinant, the characteristic equation can be obtained as

$$\lambda^2 + 2A_1\lambda + A_1^2 + A_2A_3 = 0. \tag{2.21}$$

From Eq (2.21), due to $A_1 = \frac{C(q)}{2} > 0$, the stability condition for the steady-state solution is

$$A_1^2 + A_2A_3 > 0. \tag{2.22}$$

This condition shows that when there are three solution branches in the amplitude-frequency equation, the median solution branch is unstable.

3. Analysis of amplitude-frequency characteristics

In this section, through a comparative analysis of the amplitude-frequency curves of the system's primary resonance under varying parameters, the patterns of how each parameter influences the

system's vibration state can be deduced. Specifically, by examining the changes in resonance amplitude and frequency across different values of fractional order q, damping coefficient μ, and pulse pressure F, we aim to clarify their quantitative and qualitative effects on the dynamic behavior of the fractional-order coronary artery model. This analysis helps reveal how physiological/pathological factors (e.g., arterial wall elasticity, blood viscosity, blood pressure fluctuations) modulate resonance characteristics, providing a theoretical basis for understanding cardiovascular dynamics and potential spasm mechanisms.

3.1. Bifurcations of primary resonance

In our study of the fractional-order coronary artery model, this section focuses on the bifurcations of the primary resonance for a given set of parameters with $\omega = 1.2$. The key parameters within the model play a decisive role in shaping the system's behavior. Specifically, by leveraging the analytical solution of Eq (2.16), we can systematically deduce how the resonance amplitude behaves as each parameter of the system varies independently. Moreover, based on Eq (2.18), we can draw a significant conclusion regarding the primary resonance. The peak value of the primary resonance is closely related to the amplitude of the pulse F, the natural frequency ω, and the order of fractional-order derivative q. The peak value of the primary resonance trends to increase along with an increasing F and a decreasing $|\mu\omega^{q-1}\sin(\frac{q\pi}{2})|$. The obtained results are visually presented in Figures 1 and 2. These figures are essential for understanding how different parameter variations affect the resonance amplitude in the coronary artery model. The fractional damping coefficient μ is of particular interest, as its fluctuations can modify the energy-storage and dissipation characteristics of the arterial wall, thereby directly influencing the resonance amplitude.

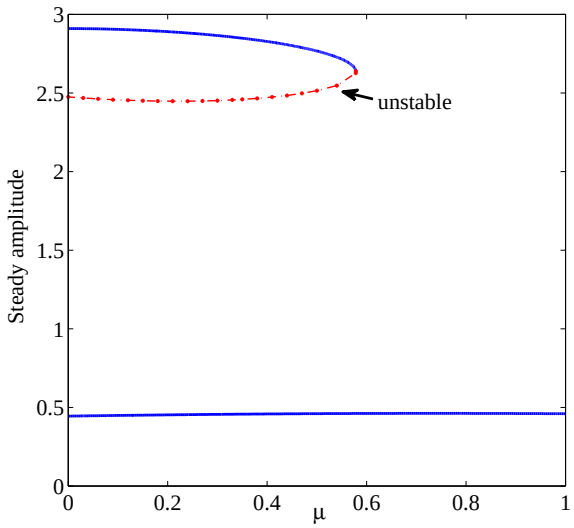

Figure 1. Resonant amplitude with μ for $q = 0.9$, $F = 0.3$, $\omega = 1.2$.

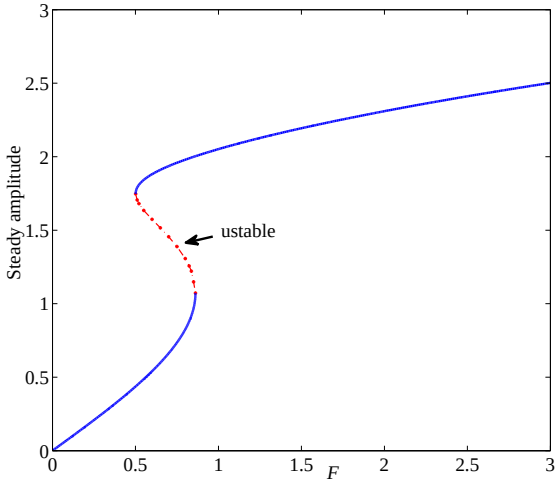

Figure 2. Resonant amplitude with F for $q = 0.9$, $\mu = 0.3$, $\omega = 1.2$.

The unstable region within the model is determined using Eqs (2.21) and (2.22). A detailed examination of the associated graphs reveals the presence of multi-solutions and a jump phenomenon. In the context of the coronary artery model, this indicates that under specific parameter combinations, the system is capable of manifesting various stable states, with sudden transitions occurring between them. Notably, our analysis confirms that the intermediate solution is unstable. This instability may potentially be linked to the emergence of abnormal blood flow patterns, such as those observed during coronary artery spasm or other cardiovascular dysfunctions.

In summary, a comprehensive understanding of these bifurcation behaviors is not only essential for unravelling the intricate dynamics of the coronary artery system but also provides valuable insights for future research on cardiovascular diseases. Such knowledge deepens our comprehension of the underlying mechanisms and can guide the development of more effective diagnostic and therapeutic strategies.

3.2. Influence of parameters on the fractional-order model

Based on Eq (2.16), we can explore the impact of several key parameters on the amplitude-frequency curve. In the context of our coronary artery model, we focus on the effects of the fractional order q, damping coefficient μ, and pulse pressure F. When these parameters vary, the corresponding results are presented in Figures 3–5, respectively.

For Figure 3, the specific parameter values are set as $\alpha = 1$, $\mu = 0.3$, $\gamma = 1$, and $F = 0.3$. The fractional differential term's behavior varies with the fractional order q. When q approaches 0, the fractional differential term approximates linear stiffness, while when q approaches 1, it behaves more like linear damping. These theoretical properties have significant real-world implications for cardiovascular health. Arterial stiffness, analogous to the state when q nears 0, is linked to aging, hypertension, and atherosclerosis, which can increase the heart's workload and raise the risk of heart failure or stroke. Damping behavior, prominent as q approaches 1, affects the artery's energy dissipation during blood flow; reduced damping can lead to abnormal blood pressure fluctuations.

Figure 3 also shows that a smaller q value results in a larger system maximum amplitude, with the integer-order model yielding the lowest amplitude. This indicates that past integer-order models

may have underestimated risks. In medicine, the fractional-order model enables more accurate assessment of arterial damage, guiding earlier interventions for patients with coronary artery diseases. Using a constitutive model calibrated for coronary arteries, which considers their viscoelastic and fractional-order properties, is essential for analyzing dynamic stability. In medical device development, integrating these properties into stents and artificial blood vessels can enhance performance, reducing restenosis risk and improving patient outcomes.

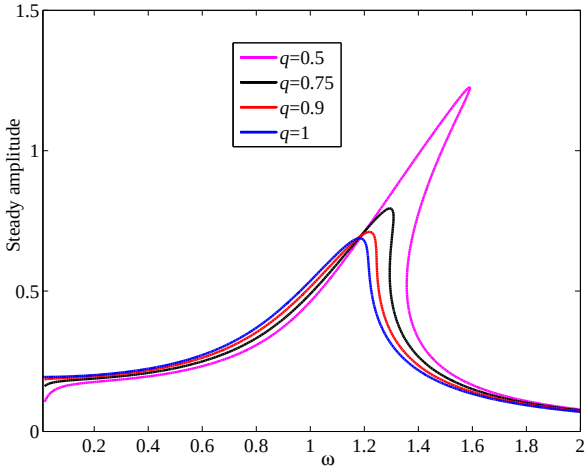

Figure 3. Effect of the fractional order q on the amplitude-frequency curves.

In Figure 4, the parameters are set as $q = 0.9$, $\alpha = 1$, $\gamma = 1$, and $F = 0.3$. From an analysis of Figure 4, it becomes evident that in the coronary artery model, as the damping coefficient μ decreases, the amplitude of the system increases. This increase in amplitude is particularly significant in the context of the coronary artery, as it implies a higher likelihood of irregular blood flow patterns. Specifically, a higher amplitude can lead to an elevated risk of coronary artery spasm. This is because the reduced damping fails to adequately regulate the oscillatory behavior of the arterial system, potentially causing the artery to contract spasmodically.

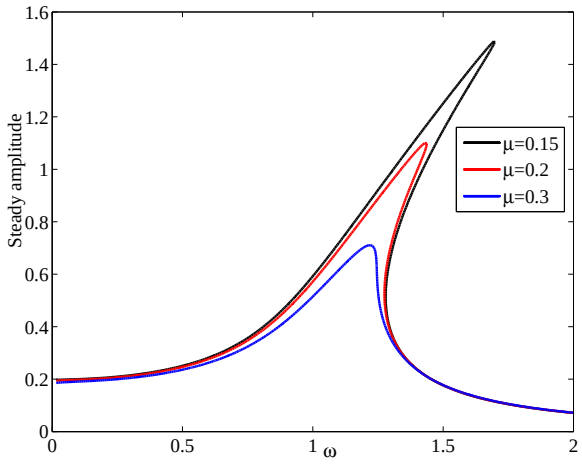

Figure 4. Effect of the fractional damping coefficient μ on the amplitude-frequency curves.

In medical device design, understanding this relationship is crucial. For example, when developing stents, engineers can adjust the material properties to mimic appropriate damping coefficients. Stents with optimized damping can better stabilize arterial oscillations, reducing the likelihood of amplitude-induced complications and improving long-term patency rates. Similarly, in the creation of artificial hearts or assist devices, accurately modeling damping coefficients based on Figure 4 insights can enhance blood flow regulation, ensuring more physiological operation and patient safety.

The impact of pulse pressure F on the amplitude-frequency curve is illustrated in Figure 5, where the fractional order is maintained at $q = 0.9$. The other parameters in Figure 5 are $\alpha = 1$, $\mu = 0.3$, and $\gamma = 1$. According to the data presented in this figure, a clear relationship emerges: Larger values of F result in a larger maximum amplitude. This finding aligns well with real-world observations. In clinical practice, coronary artery spasm is more prevalent in individuals with certain risk factors, such as smokers, those with high cholesterol, or those with high blood pressure. High blood pressure, which is related to increased pulse pressure, is indeed associated with an increased likelihood of coronary artery spasm.

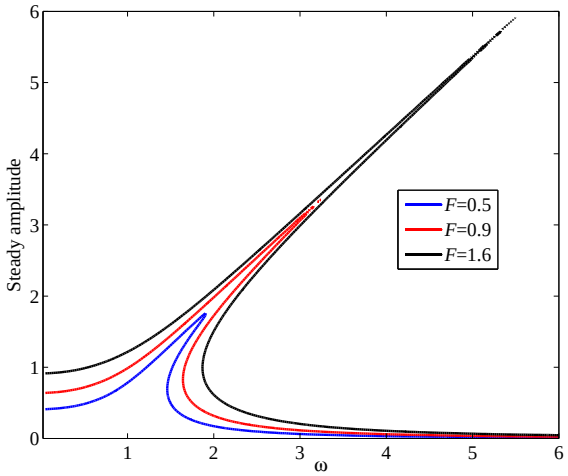

Figure 5. Effect of the pulse pressure F on the amplitude-frequency curves.

In the clinical treatment of coronary artery spasm, strict blood pressure control is of utmost importance. Nitroglycerin, a vasodilator drug first approved in 2000, plays a crucial role in this regard. Nitroglycerin acts on vascular smooth muscle, causing it to relax and leading to the dilation of both arteries and veins. By doing so, it effectively reduces cardiac preload and afterload, alleviates coronary artery spasm. The reduction in cardiac work achieved by nitroglycerin is considered the primary mechanism through which it relieves angina pectoris symptoms. Additionally, its ability to dilate small arteries further contributes to improving blood flow and reducing the risk of coronary artery spasm [33].

It should be pointed out that, in clinical practice, the acquisition of accurate parameters for the fractional-order coronary artery model requires sophisticated measurements of arterial wall properties and hemodynamic data, such as viscoelastic modulus, fractional order q, and pulse pressure F, which currently face significant challenges. Direct clinical measurement of these parameters demands high-resolution imaging techniques and specialized mechanical testing, which are not yet routinely available in standard diagnostic settings. Additionally, individual variations in coronary artery structure and

function across patients further complicate parameter calibration. To address this, the parameters used in this study are selected primarily for illustrative purposes to demonstrate the model's theoretical behavior and parameter influence trends, rather than reflecting precise physiological values. While these values are inspired by simplified mechanical analogs and existing literature, they require validation through future clinical experiments.

4. Comparison between the approximate analytical solution and numerical solution

According to Eq (2.16), the primary resonance amplitude-frequency response curve of the system can be drawn. For comparison, this paper adopts the power series method introduced in references [34, 35], and its calculation formula is

$$D^q_{t_n}[y(t_n)] \approx h^{-q} \sum_{j=0}^{n} C^q_j y(t_{n-j}), \tag{4.1}$$

where $t_n = nh$ are the sample points, h is the sample step, and C^q_j is the fractional binomial coefficient with the iterative relationship

$$C^q_0 = 1, \quad C^q_j = (1 - \frac{1+q}{j})C^q_{j-1}. \tag{4.2}$$

According to Eqs (4.1) and (4.2), the numerical scheme for Eq (2.3) can be expressed as

$$x(t_n) = y(t_{n-1})h - \sum_{j=1}^{n} C^1_j x(t_{n-j}), \tag{4.3a}$$

$$y(t_n) = [F\cos(\omega t_n) - \alpha x(t_n) - \gamma x^3(t_n) - \mu z(t_{n-1})]h - \sum_{j=1}^{n} C^1_j y(t_{n-j}), \tag{4.3b}$$

$$z(t_n) = y(t_n)h^{1-q} - \sum_{j=1}^{n} C^{1-q}_j z(t_{n-j}). \tag{4.3c}$$

All the parameter values in (2.3) should be identified from measurements of periodic motion of the blood circulation system, but they are currently not available. For simplicity, the selection of parameters is referred to [28–30], which needs further experimental support. The sample step is set as $h = 0.005$, and the total computation time is 150 s. After omitting the temporary response in frontal 60 s, the peak value of the posterior response is taken as the steady-state amplitude by the numerical results.

Based on Eq (2.16), the amplitude-frequency response curve can be obtained analytically, as shown in Figure 6. According to Eqs (4.3a)–(4.3c), the amplitude-frequency response can be obtained by numerical integration, which is also shown in Figure 6 and represented by a circle. The parameter settings for the analysis are provided in two sets: (a) With $q = 0.84$, $\alpha = 1$, $\mu = 0.2$, $\gamma = 0.1$, and $F = 0.1$; (b) with $q = 0.85$, $\alpha = 1$, $\mu = 0.3$, $\gamma = 1$, and $F = 0.2$. Upon careful examination of Figure 6, it becomes evident that the approximate analytical solution shows a high degree of consistency with the numerical results. This agreement validates the effectiveness and reliability of the analytical approaches employed in this study.

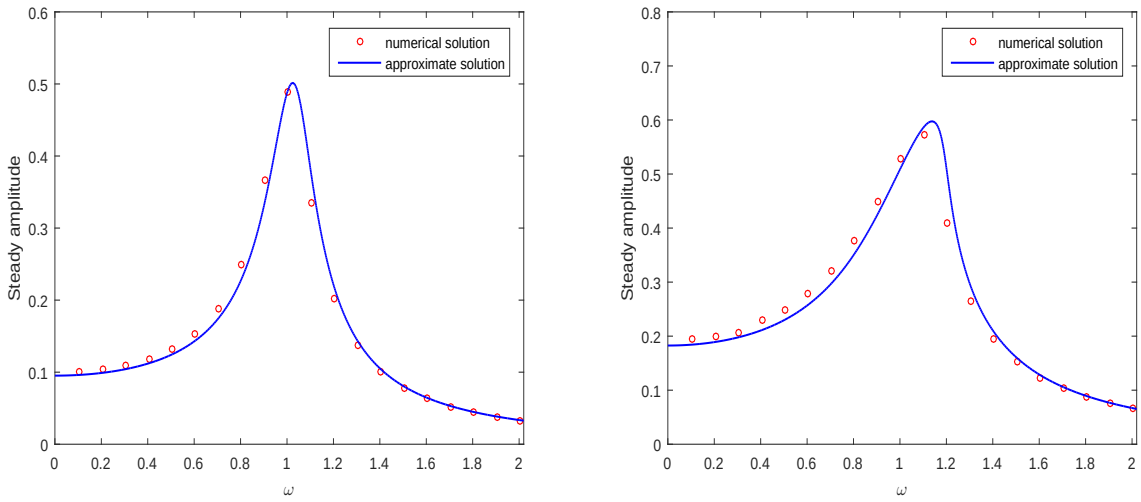

(a) (b)

Figure 6. Comparison between the approximate analytical solution and numerical solution.

5. Conclusions

From the above-mentioned results, it is evident that the fractional order and the fractional damping coefficient play crucial roles in the fractional-order coronary artery model. For instance, an increase in both the fractional order and the fractional damping coefficient can effectively reduce the resonance's effective amplitude and modify the resonance frequency. This finding is instructive when it comes to selecting or designing appropriate fractional parameters for controlling blood vibrations within the coronary artery model. In addition to the fractional-related parameters, factors such as blood flow resistance, the elasticity of the vessel wall, and pulse pressure also significantly influence the model's results. A large pulse pressure, in particular, will cause an elevation in the resonance amplitude. In a real-world context, this corresponds to the phenomenon where fluctuations in blood pressure may trigger coronary artery spasms, which can have serious implications for cardiovascular health.

Notably, coronary artery primary resonance is linked to disease pathogenesis: Resonance-induced high stress/strain damages vessel walls, promoting atherosclerotic plaques, while turbulent flow exacerbates narrowing and triggers heart attacks. Studying resonance in fractional-order models reveals mechanical mechanisms, inspiring new diagnostic and therapeutic approaches—such as modifying arterial elasticity or reducing external disturbances to prevent resonance and curb disease progression. While model parameter selection relies on medical experiments, this study provides theoretical insights. Optimizing parameters based on clinical trials is a critical topic, requiring collaboration between theorists and medical professionals to advance the model's medical application. Moving forward, integrating patient-specific parameters with clinical data will refine the model, enhancing its accuracy and clinical relevance to bridge theoretical modeling with personalized cardiovascular diagnostics and treatments.

Author contributions

Guanghua Wei: Writing–original draft, writing–review and editing; Xiaorong Zhang: Investigation, validation; Zhoujin Cui: Conceptualization, methodology, validation, supervision. All authors have read and approved the final version of the manuscript.

Use of Generative-AI tools declaration

The authors declare they have not used Artificial Intelligence (AI) tools in the creation of this article.

Acknowledgments

The authors express gratitude to the reviewers and editors for their helpful comments and suggestions, as well as for the financial support from the Research Foundation of Jinling Institute of Technology (No. jit-b-202206) and the High Level Talent Research Launch Fund of Jiangsu Second Normal University (No. 928201/058).

Conflict of interest

All authors declare no conflict of interest in this paper.

References

1. Cardiovascular diseases (CVDs), Available from: https://www.who.int/en/news-room/fact-sheets/detail/cardiovascular-diseases-(cvds).
2. D. M. Wootton, D. N. Ku, Fluid mechanics of vascular systems, diseases, and thrombosis, *Annu. Rev. Biomed. Eng.*, **1** (1999), 299–329. https://doi.org/10.1146/annurev.bioeng.1.1.299
3. A. El-Gohary, Chaos and optimal control of cancer self-remission and tumor system steady states, *Chaos Soliton. Fract.*, **37** (2008), 1305–1316. https://doi.org/10.1016/j.chaos.2006.10.060
4. W. Zhang, L. Pei, Bifurcation and chaos in N-type and S-type muscular blood vessel models, *Electro. Res. Arch.*, **33** (2025), 1285–1305. https://doi.org/10.3934/era.2025057
5. G. Meng, X. Zong, Periodic solution of mathematical model of muscular blood vessel, *J. Yangzhou Univ. Nat. Sci.*, **3** (2000), 15–19. https://doi.org/10.3969/j.issn.1007-824X.2000.02.004
6. C. Lin, S. Yang, H. Yau, Chaos suppression control of a coronary artery system with uncertainties by using variable structure control, *Comput. Appl. Math.*, **64** (2012), 988–995. https://doi.org/10.1016/j.camwa.2012.03.007
7. A. Karimi, R. Razaghi, M. Koyama, A patient-specific numerical modeling of the spontaneous coronary artery dissection in relation to atherosclerosis, *Comput. Meth. Prog. Bio.*, **182** (2019), 105060. https://doi.org/10.1016/j.cmpb.2019.105060
8. V. Carvalho, D. Pinho, R. A. Lima, J. C. Teixeira, S. Teixeira, Blood flow modeling in coronary arteries: A review, *Fluids*, **6** (2021), 53. https://doi.org/10.3390/fluids6020053

9. H. Ding, D. Qian, S. Lee, L. Zhu, Sliding-mode-based chaos suppression of coronary artery systems, *Meas. Control*, **56** (2023), 1684–1693. https://doi.org/10.1177/00202940231180842
10. G. El Khaloufi, N. Chaibi, S. B. Alaoui, I. Boumhidi, Generalized dissipativity dynamic output feedback control for coronary artery system, *T. I. Meas. Control*, **46** (2024), 716–728. https://doi.org/10.1177/01423312231182177
11. D. Craiem, F. Rojo, J. Atienza, G. Guinea, R. L. Armentano, Fractional calculus applied to model arterial viscoelasticity, *Lat. Am. Appl. Res.*, **38** (2008), 141–145. https://doi.org/10.1016/j.supflu.2007.12.004
12. D. Craiem, F. J. Rojo, J. M. Atienza, R. L. Armentano, G. V. Guinea, Fractional-order viscoelasticity applied to describe uniaxial stress relaxation of human arteries, *Phy. Med. Biol.*, **53** (2008), 4543. https://doi.org/10.1088/0031-9155/53/17/006
13. Y. Yu, P. Perdikaris, G. E. Karniadakis, Fractional modeling of viscoelasticity in 3D cerebral arteries and aneurysms, *J. Comput. Phys.*, **323** (2016), 219–242. https://doi.org/10.1016/j.jcp.2016.06.038
14. C. Ionescu, A. Lopes, D. Copot, J. A. T. Machado, J. H. T. Bates, The role of fractional calculus in modeling biological phenomena: A review, *Commun. Nonlinear Sci.*, **51** (2017), 141–159. https://doi.org/10.1016/j.cnsns.2017.04.001
15. Z. Cui, Z. Wang, Primary resonance of a nonlinear fractional model for cerebral aneurysm at the circle of Willis, *Nonlinear Dynam.*, **108** (2022), 4301–4314. http://dx.doi.org/10.1007/s11071-022-07445-z
16. A. Ranjbar, A. Madady, M. Ramezani, A. Khosravi, Synchronization of stochastic fractional-order model of muscular blood vessels, *J. Vib. Control*, **30** (2024), 3775–3783. https://doi.org/10.1177/10775463231201732
17. M. P. Aghababa, M. Borjkhani, Chaotic fractional-order model for muscular blood vessel and its control via fractional control scheme, *Complexity*, **20** (2015), 37–46. https://doi.org/10.1002/cplx.21502
18. Z. Wang, M. Du, symptotical behavior of the solution of a SDOF linear fractionally damped vibration system, *Shock Vib.*, **18** (2011), 257–268. https://doi.org/10.3233/SAV-2010-0566
19. Y. Shen, S. Yang, H. Xing, G. Gao, Primary resonance of Duffing oscillator with fractional-order derivative, *Commun. Nonlinear Sci.*, **17** (2012), 3092–3100. https://doi.org/10.1016/j.cnsns.2011.11.024
20. Y. Shen, S. Wen, X. Li, S. Yang, H. Xing, Dynamical analysis of fractional-order nonlinear oscillator by incremental harmonic balance method, *Nonlinear Dynam.*, **85** (2016), 1457–1467. https://doi.org/10.1007/s11071-016-2771-8
21. S. Li, J. Niu, X. Li, Primary resonance of fractional-order Duffing-van der Pol oscillator by harmonic balance method, *Chinese Phys. B*, **27** (2018), 120502. https://doi.org/10.1088/1674-1056/27/12/120502
22. Z. Cui, G. Wei, T. Lu, Simultaneous resonance analysis of a fractional cerebral aneurysm model with double-frequency excitation, *J. Vib. Eng. Technol.*, **13** (2025), 23. https://doi.org/10.1007/s42417-024-01566-y

23. G. Alotta, M. D. Paola, F. P. Pinnola, An unified formulation of strong non-local elasticity with fractional order calculus, *Meccanica*, **57** (2022), 793–805. https://doi.org/10.1007/s11012-021-01428-x

24. R. L. Magin, Fractional calculus models of complex dynamics in biological tissues, *Comput. Math. Appl.*, **59** (2010), 1586–1593. https://doi.org/10.1016/j.camwa.2009.08.039

25. A. H. Nayfeh, D. T. Mook, *Nonlinear oscillations*, New York: Wiley-Interscience, 1995. https://doi.org/10.1002/9783527617586

26. J. A. Sanders, F. Verhulst, J. Murdock, *Averaging methods in nonlinear dynamical systems*, New York: Springer, 2007. https://doi.org/10.1007/978-0-387-48918-6

27. V. Burd, *Method of averaging for differential equations on an infinite interval: Theory and applications*, New York: Taylor & Francis Group, 2007. https://doi.org/10.1201/9781584888758

28. Z. Zhao, J. Zhang, G. Ding, D. Zhang, Chaos synchronization of coronary artery system based on higher order sliding mode adaptive control, *Acta Phys. Sin.*, **64** (2015), 1–8. https://doi.org/10.7498/aps.64.210508

29. C. Gong, Y. Li, X. Sun, Backstepping control of synchronization for biomathematical model of muscular blood vessel, *J. Appl. Sci.*, **24** (2006), 604–607. https://doi.org/10.3969/j.issn.0255-8297.2006.06.012

30. P. Roy, S. Ray, S. Bhattacharya, *Synchronization of two chaotic coronary artery systems using modified feedback method*, In: International Conference on Control, Instrumentation, Energy and Communication, IEEE, 2016, 145–148. https://doi.org/10.1109/CIEC.2016.7513819

31. J. P. Lasalle, *The stability of dynamical systems*, Phila: Society for Industrial and Applied Mathematics, 1976. https://doi.org/10.1137/1.9781611970432

32. G. Meng, Approximation solutions in the biomathematical model of muscular blood vessel (ii), *J. Yangzhou Univ. Nat. Sci.*, **5** (2002), 18–20. https://doi.org/10.3969/j.issn.1007-824X.2002.01.005

33. K. H. Kim, C. C. Adnan, D. J. Schaller, *Nitroglycerin*, StatPearls Publishing, 2023.

34. R. Caponetto, G. Dongola, L. Fortuna, I. Petras, *Fractional order systems: Modeling and control applications*, World Scientific, 2010. https://doi.org/10.1142/7709

35. I. Petras, *Fractional-order nonlinear systems: Modeling, analysis and simulation*, Heidelberg: Springer Berlin, 2011. http://dx.doi.org/10.1007/978-3-642-18101-6

AIMS Press